JOURNAL OF MATERIALS SCIENCE 29 (1994) 851-860

Elevated-temperature deformation properties of a HfC modified Ti–48Al–2Mn–2Nb matrix particulate composite

J. D. WHITTENBERGER, S. C. FARMER, D. A. BORS*
*NASA Lewis Research Center, and * Calspan Corporation, NASA Lewis Research Center, Cleveland, OH 44135, USA*

R. RAY
Marko Materials Inc., North Billerica, MA 01862, USA

D. S. LEE
Materials Laboratory, Wright Patterson Air Force Base, OH 45433, USA

Rapid solidification techniques in combination with HIPing have been used to produce Ti–48Al–2Mn–2Nb and a Ti–48Al–2Mn–2Nb+15 wt% HfC composite. While the composite does contain several second phases within the $\gamma + \alpha_2$ matrix, none was identified to be HfC. The elevated-temperature properties were determined by constant velocity compression and constant load tensile testing in air between 1000 and 1173 K. Such testing indicated that the elevated temperature strengths of the HfC-modified aluminide was superior to those of the unreinforced matrix with the best 1100 K temperature slow strain rate properties for both materials being achieved after high-temperature annealing prior to testing. Examination of the microstructures after deformation in combination with the measured stress exponents and activation energies suggest that creep resistance of the HfC-modified form is due to solid-solution strengthening from carbon and hafnium rather than the presence of second phases.

1. Introduction

The intermetallic phase TiAl (γ) has been studied for approximately 40 years as a possible low-density replacement for superalloys [1] in aerospace applications. For example, Allen *et al.* [2] have determined that the use of titanium-based materials (density of $\sim 4\ \mathrm{Mg\,m^{-3}}$) in place of a Ni_3Al-strengthened nickel-base superalloy (density of $\sim 7.9\ \mathrm{Mg\,m^{-3}}$) for a compressor system (rotor, stator and case) would result in a weight reduction of approximately 260 kg which corresponds to a 4% decrease in the overall weight of the gas turbine engine. Such reductions would directly lead to better fuel usage, hence lower operating costs over the lifetime of the engine.

To date, the vast majority of the work on TiAl has been focused on improvement of the oxidation resistance, low-temperature tensile ductility and fracture toughness, as noted in the recent review by Y.-W. Kim [1]. Most TiAl of current interest for engineering applications contain third-element additions to a base composition of Ti-48Al (at %) which possesses a two-phase microstructure consisting of α_2 (Ti_3Al) + γ. Alloying additions are generally made at the 1%–3% levels to improve oxidation resistance (i.e. niobium [3]) or low-temperature tensile ductility (i.e. manganese [4]).

Because TiAl-based materials are intended to be used at elevated temperature up to at least 1100 K, creep will become important. Hence a study (Air Force SBIR Phase I Contract F33615-90-C-5945) was funded to examine the elevated-temperature deformation resistance of discontinuous composites based on a Ti–48Al–2Mn–2Nb matrix as a means to improve the creep properties. This composition was chosen because it represents a typical two-phase titanium aluminide which has been alloyed for both tensile ductility and oxidation resistance. This paper documents the microstructure and elevated-temperature slow strain rate behaviour of this matrix and a particulate composite resulting from a 15 wt % HfC addition. All materials were made by rapid solidification techniques (RST) in combination with hot isostatic pressing (HIPing) as the densification step.

2. Experimental procedure

The RST procedures utilized by Marko Materials, Inc. to produce Ti–48Al–2Mn–2Nb-based composites have been described previously [5, 6]. Briefly, a non-consumable tungsten arc was used to supply the energy required to melt high-purity (> 99.9%) Al, Ti, Mn, Nb and HfC in the correct proportions under an argon atmosphere. Because molten TiAl is very reactive and will attack most crucible materials, a cold-hearth technique was used to contain the liquid solution. To ensure alloy homogeneity, each material

0022–2461

was melted, frozen, turned over and remelted several times. Rapid solidification was achieved by tipping the hearth and allowing a fine stream of the melt to contact a rapidly rotating molybdenum wheel. This procedure typically yielded $\sim 40\ \mu m$ diameter, long filaments which were subsequently pulverized under argon into powder in a hammer mill. The powders were then cold compacted into titanium cans, evacuated at 670 K and sealed. Consolidation to full density was accomplished by hot isostatic pressing at 1550 K and 207 MPa for 6 h. A composite containing 15 wt % HfC in a nominally Ti–48Al–2Mn–2Nb matrix, as well as the unreinforced matrix itself, were produced in this manner.

Cylindrical test specimens, 10 mm long with a 5 mm diameter, were prepared by electrodischarge machining and grinding. Constant velocity compression tests at speeds ranging from 2.12×10^{-3}–$2.12 \times 10^{-6}\ mm\ s^{-1}$ were conducted in a universal testing machine at 1000 and 1100 K in air at the Lewis Research Center. Autographically recorded load–time charts were then converted to true compressive stresses, strains, and strain rates via the offset method and the assumption of conservation of volume. Additional details about the compression test procedures can be found elsewhere [7, 8]. To confirm that compression testing yielded a good estimate of the strength properties, several tensile creep rupture tests were conducted in air between 1033 and 1173 K on button head, 2.3 mm diameter by 10 mm gauge length specimens at the Joliet Metallurgical Laboratories, Joliet, IL.

Because the grain size of the as-HIPed materials was relatively small, samples of each composition were annealed in argon for 48 h at 1573 K. Constant velocity compression testing at 1100 K was undertaken in air on specimens given such a heat treatment to determine if grain growth led to an improvement in creep resistance.

The as-HIPed and heat-treated materials and selected tested specimens were examined by light optical, scanning electron (SEM) and transmission electron (TEM) microscopy. Standard metallurgical polishing techniques were used to prepare mounted specimens with Kroll's reagent being used for etching. TEM samples were prepared by electropolishing, utilizing Blackburn's solution of methanol, *n*-butyl alcohol and perchloric acid as the electrolyte.

3. Results

3.1. As-HIPed materials

Fig. 1 illustrates the light optical and SEM level structure of the as-HIPed materials. Ti–48Al–2Mn–2Nb possessed a twinned microstructure consisting of approximately 20 μm grain size with isolated regions of exaggerated grain growth (Fig. 1a). Use of back-scattered electron imaging in the SEM demonstrated that the matrix was a two-phase mixture (Fig. 1b), where

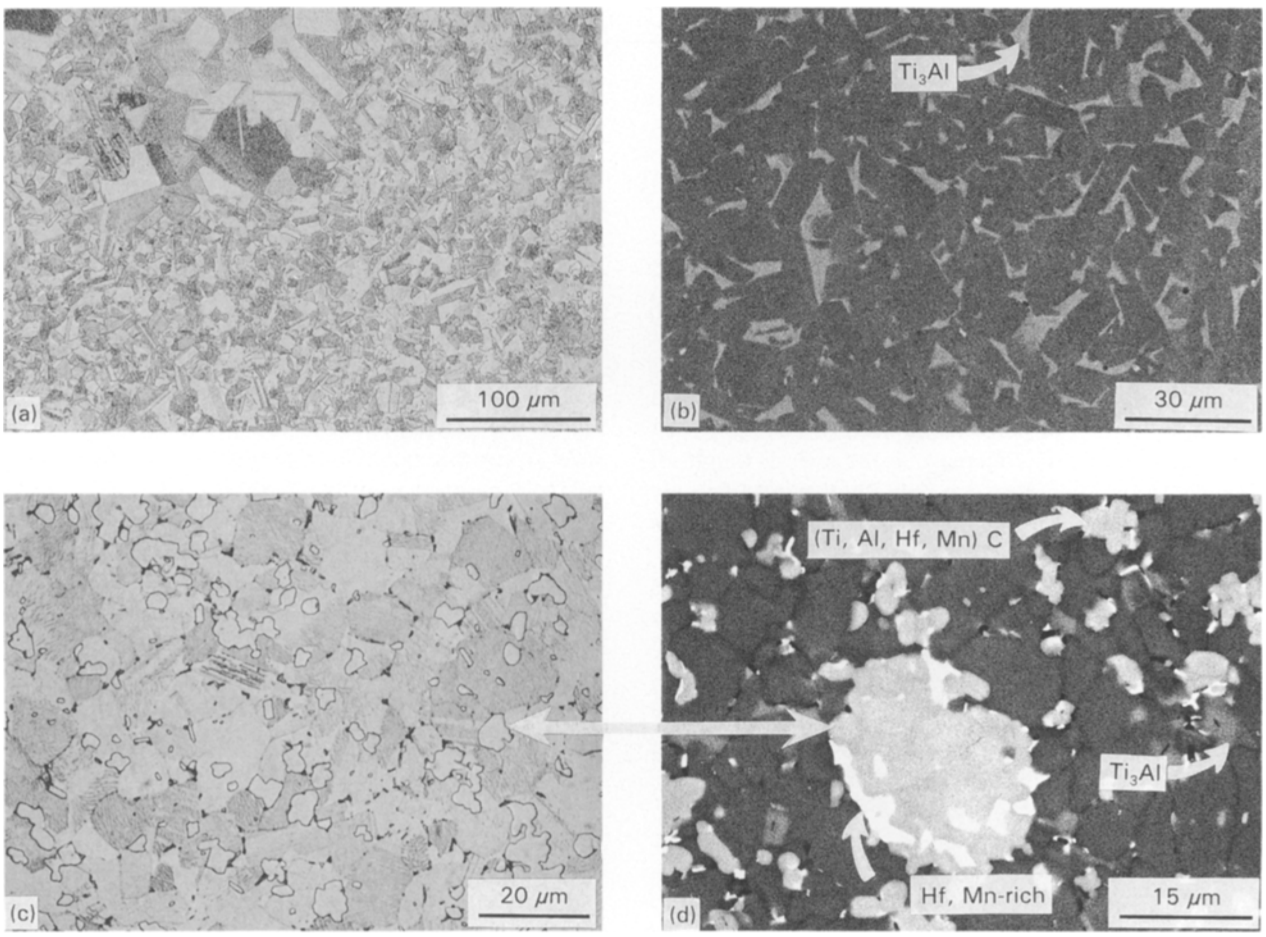

Figure 1 (a, c) Light optical and (b, d) scanning electron micrographs of as-HIPed (a, b) Ti–48Al–2Mn–2Nb and (c, d) Ti–48Al–2Mn–2Nb + 15 wt % HfC.

the light grey phase is titanium-rich. Electron diffraction analysis in a TEM positively identified the presence of TiAl grains and Ti_3Al at the boundaries. While occasional α_2 laths were seen during TEM study, no regions of extended lamellar morphology were observed. The addition of 15 wt % HfC to the matrix produced about a factor of two refinement in the grain size as well as a globular second phase (Fig. 1c). Energy dispersive analysis of this phase in an SEM, in combination with TEM electron diffraction analysis, indicated that it was a titanium aluminium carbide containing hafnium and niobium. Further examination of the HfC-modified composite verified the existence of four distinct phases (Fig. 1d) including gamma (darkest contrast), globular alpha-2 (dark grey), a Hf, Mn-enriched phase (white) and the light grey carbide which is the visible second phase in Fig. 1c. While both TiAl and Ti_3Al also contained hafnium, no evidence for HfC was found. Apparently this carbide is completely dissolved during the initial melting preceding spinning, and it never reforms during solidification or subsequent solid-state processing. Therefore, it is likely that the matrix contains carbon in addition to hafnium.

TEM examination of Ti–48Al–2Mn–2Nb indicated that numerous dislocations and subboundaries (Fig. 2a) existed in the as-HIPed microstructure. A study of the composite in regions away from the large precipitates (Fig. 2b) indicated that the $\gamma + \alpha_2$ matrix contained very few small second-phase particles or dislocations.

3.2. As-HIPed mechanical properties

True compressive stress–strain diagrams determined for the as-HIPed matrix and HfC-modified composite at 1000 and 1100 K are presented in Figs 3 and 4 as functions of the nominal strain rate. Rapid work hardening was observed over the first $\sim 1\%$ strain for all materials and test conditions. Beyond this level of deformation, the behaviour was not uniform, and examples of continuous but slow strain hardening, flow at a more or less constant stress, and even slight strain softening can be found. Comparison of the two materials compressed under like circumstances indicates that the addition of HfC to the matrix can yield about a 60% improvement in the 1000 K strength (Figs 3a and 4a). Except for the test at a strain rate of $\sim 2 \times 10^{-6}\ s^{-1}$, which only demonstrated a 35% improvement, the 1100 K strength of the HfC-modified material (Fig. 4b) also maintained an $\sim 60\%$ increase over that of the matrix (Fig. 3b).

Results from the tensile creep tests on as-HIPed Ti–48Al–2Mn–Nb and Ti–48Al–2Mn–Nb + 15 wt % HfC are shown in Fig. 5, and the failure time and measures of ductility are given in Table I. While the 1033 K, 206.9 MPa test for Ti–48Al–2Mn–Nb + 15 wt % HfC (Fig. 5b) possessed a normal creep curve (pronounced first-stage creep followed by steady state), behaviour of all the other tests can be characterized by the almost immediate transition into second- and third-stage creep with most of the deformation in the tertiary regime. Comparison of the stress–temperature–life data in Table I for both materials indicates that the addition of 15 wt % HfC to the Ti–48Al–2Nb–2Mn matrix does improve the elevated temperature strength. Additionally, the measures of ductility at rupture signify that tensile creep deformation of both materials is relatively uniform and that the particulates are not reducing the plasticity of the matrix.

True flow stress, σ – strain rate, $\dot{\varepsilon}$, behaviour for the as-HIPed Ti–48Al–2Mn–2Nb materials are presented in Fig. 6, where tensile and compressive data were intermingled by treating both σ and $\dot{\varepsilon}$ as absolute quantities. The flow stresses and strain rates were evaluated at 1% strain from the compression results (Figs 3 and 4), while the steady-state creep rate and average stress over the second-stage regime were utilized from the tensile creep tests (Fig. 5). The fastest

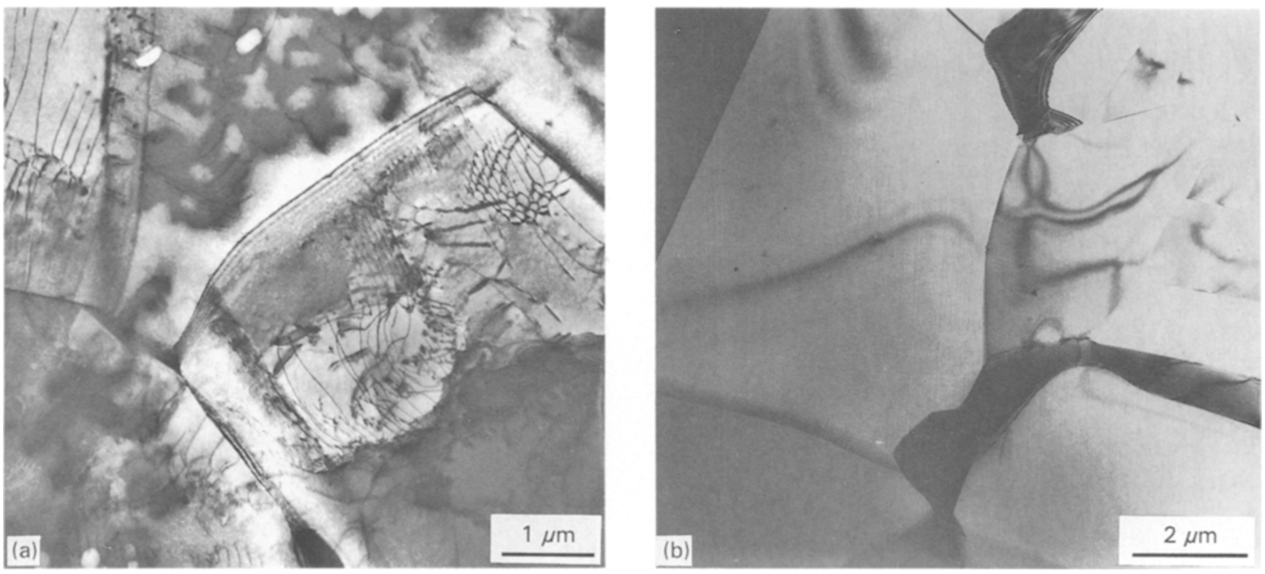

Figure 2 Transmission electron micrographs of the as-HIPed (a) Ti–48Al–2Mn–2Nb and (b) Ti–48Al–2Mn–2Nb + 15 wt % HfC.

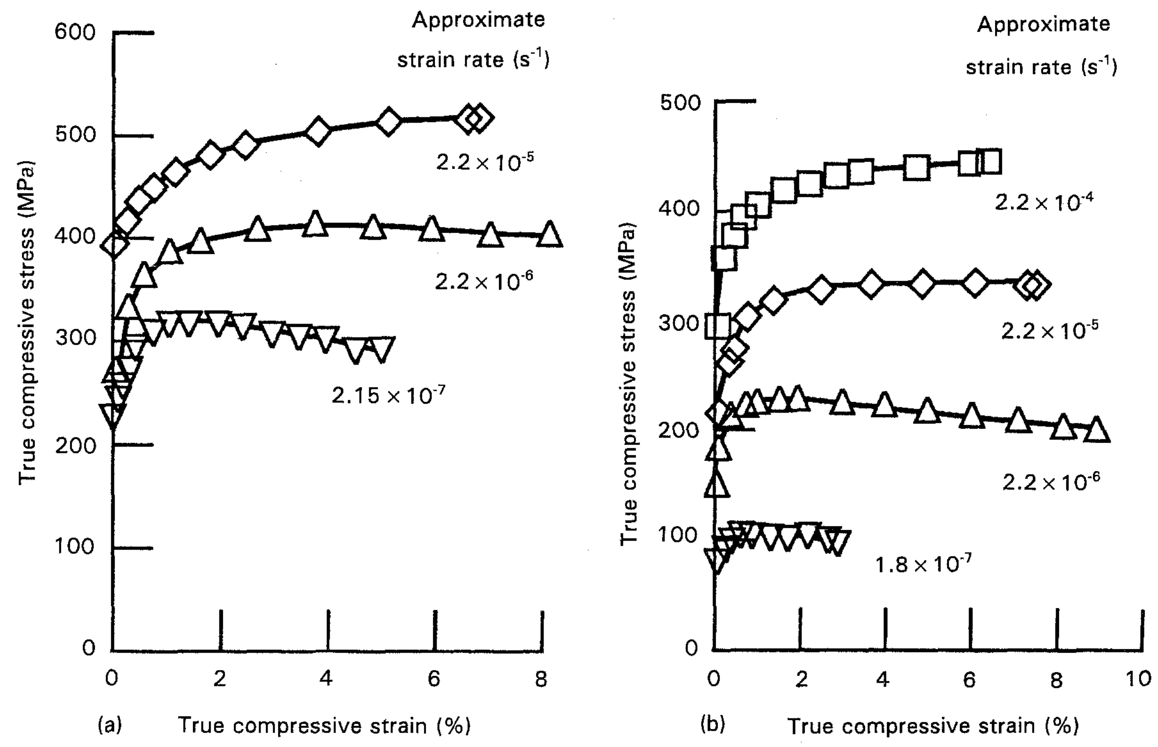

Figure 3 True compressive stress–strain diagrams for as-HIPed Ti–48Al–2Mn–2Nb tested under constant velocity conditions in air at (a) 1000 and (b) 1100 K.

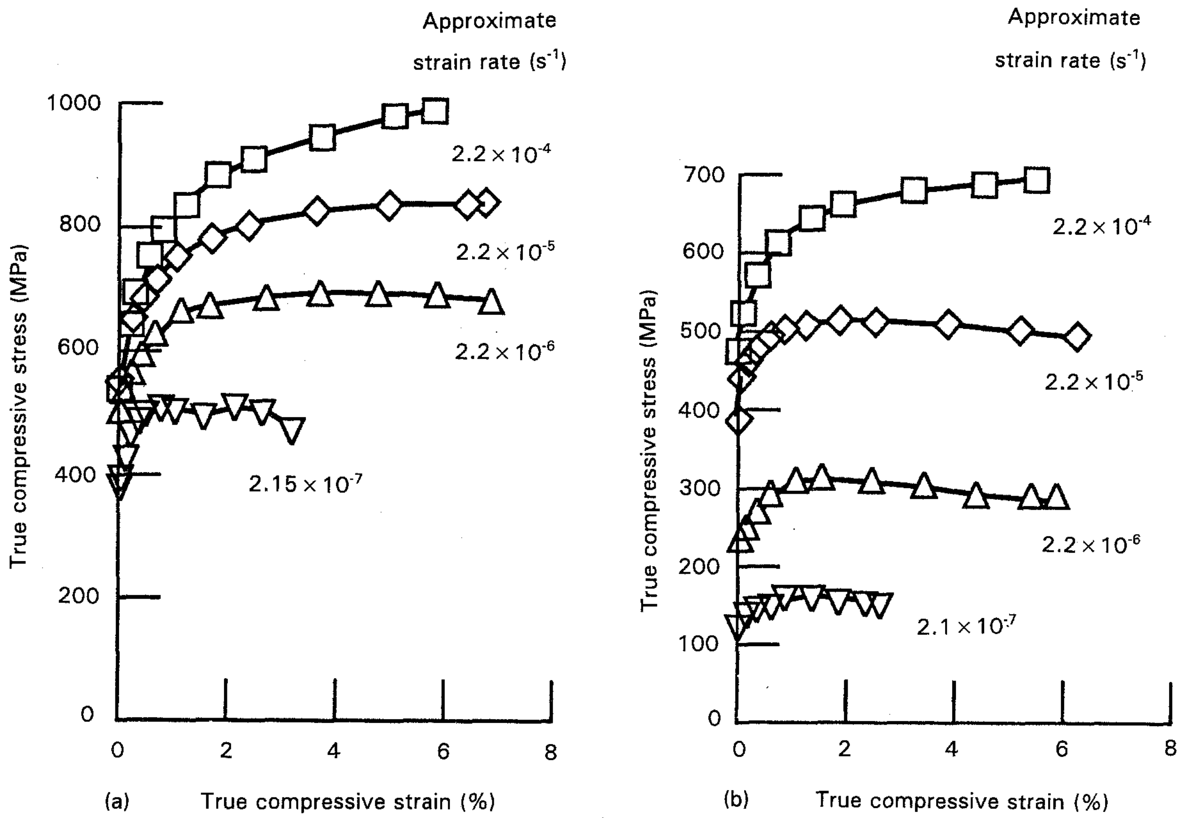

Figure 4 True compressive stress–strain diagrams for as-HIPed Ti–48Al–2Mn–2Nb + 15 wt % HfC tested under constant velocity conditions in air at (a) 1000 and (b) 1100 K.

three compression tests for Ti–48Al–2Mn–2Nb at 1000 and 1100 K were fitted to a power law equation

$$\dot{\varepsilon} = A\sigma^n \tag{1}$$

where A is a constant and n is the stress exponent. From the coefficient of determination, R_d^2, and the standard deviations for the stress exponent, δ_n, in Table II as well as visually from the curves in Fig. 6a, it is clear that Equation 1 adequately describes the data. Because both the curves and stress exponents (Table II) reveal that the deformation mechanism of as-HIPed Ti–48Al–2Mn–2Nb is different at each

TABLE I Rupture parameters for as-HIPed Ti–48Al–2Mn–2Nb and Ti–48Al–2Mn–2Nb + 15 wt % HfC

Material	Stress (MPa)	Temperature (K)	Rupture		
			Time (h)	Elongation (%)	Reduction of area (%)
Ti–48Al–2Mn–2Nb	206.9	1033	61.7[a]	5.1[b]	–
	206.9	1113	5.0	11.2	13.5
Ti–48Al–2Mn–2Nb + 15 wt % HfC	206.9	1033	108.8[a]	2.74[b]	–
	137.9	1073	306.2[a]	21.7[b]	–
	206.9	1113	18.1	20.9	22.9
	137.9	1173	9.0	32.5	33.4

[a] Test discontinued at time shown.
[b] Creep strain at time test discontinued.

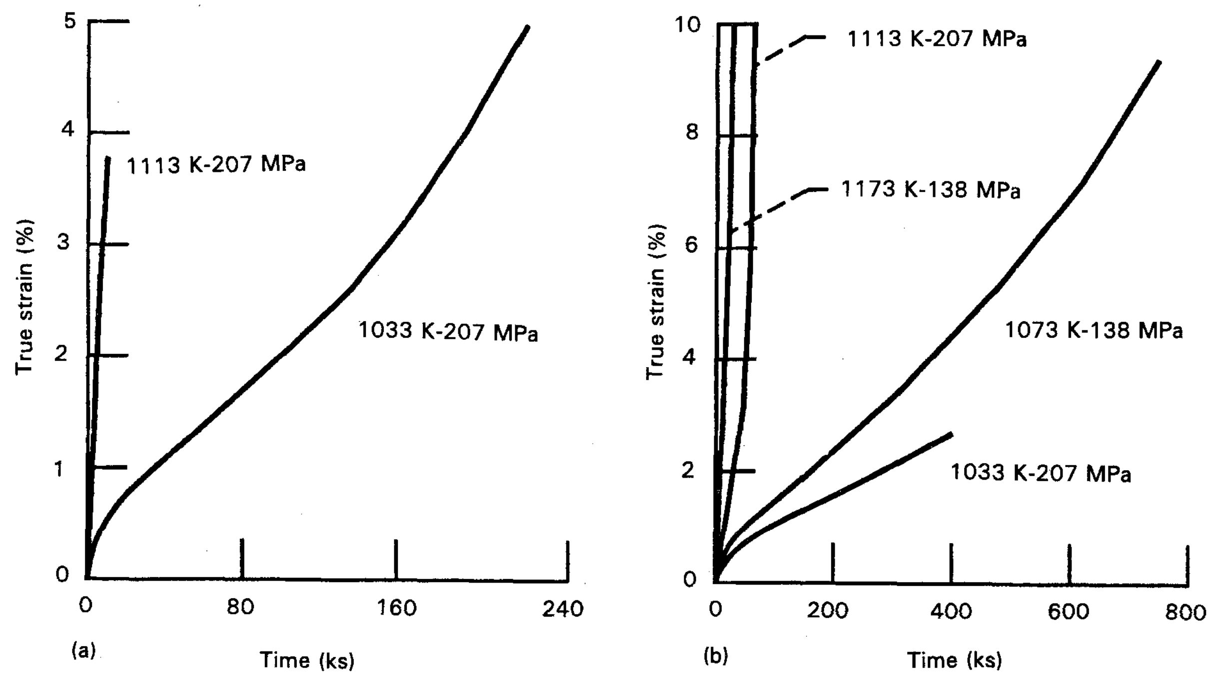

Figure 5 True strain tensile creep curves for as-HIPed (a) Ti–48Al–2Mn–2Nb and (b) Ti–48Al–2Mn–2Nb + 15 wt % HfC tested between 1033 and 1173 K.

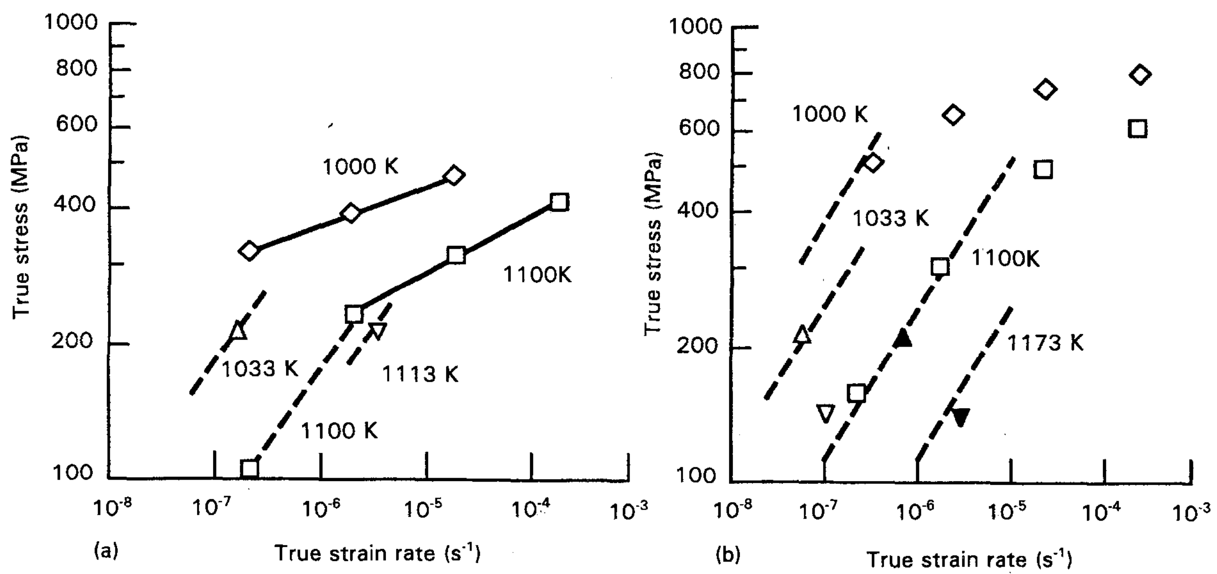

Figure 6 True flow stress–strain rate behaviour for as-HIPed (a) Ti–48Al–2Mn–2Nb and (b) Ti–48Al–2Mn–2Nb + 15 wt % HfC. (a) Compression: (◇) 1000 K, (□) 1100 K; tension: (△) 1033 K, (▽) 1113 K. (b) Compression: (◇) 1000 K, (□) 1100 K; tension: (△) 1033 K, (▽) 1073 K, (▲) 1113 K, (▼) 1173 K.

temperature, attempts to utilize these data to estimate an activation energy for deformation, Q, would not be meaningful.

With (1) the assumption that the two slowest 1100 K compression points and the tensile creep results are due to the same slow plastic deformation mechanism, and (2) the use of the standard temperature-compensated power law equation

$$\dot{\varepsilon} = B\sigma^n \exp\left(\frac{-Q}{RT}\right) \quad (2)$$

where B is a constant, R is the universal gas constant and T is the temperature, an activation energy and stress exponent for creep in the unreinforced matrix can be estimated. The appropriate regression parameters are listed in Table II along with the standard deviation, δ_Q, for the activation energy, and the resultant curves are given as dotted lines in Fig. 5a. In spite of the limited amount of data, the coefficient of determination (Table II) indicates that the assumptions and use of Equation 2 are reasonable.

Owing to the apparent curvature in the stress–strain rate data at 1000 and 1100 K for as-HIPed Ti–48Al–2Mn–Nb + 15 wt % HfC (Fig. 6b), fits to Equation 1 were not attempted. On the other hand, sufficient elevated-temperature slow strain rate results seemed to be available for employment of Equation 2. The results of this analysis are shown as dotted lines in Fig. 6b and are reported in Table II. Based on the parameters in this table, there is little difference, if any, in the deformation mechanism controlling creep in either the Ti–48Al–2Mn–Nb matrix or its HfC-modified composite.

3.3. Mechanical properties after heat treatment

Because it was probable that the fine grain size which resulted from the RST methods employed in this study might have reduced the creep resistance, both materials were annealed for 48 h at 1573 K to promote grain growth. This approach was successful for both materials where heat treatment increased the grain size from ~ 20 μm to 50 μm for Ti–48Al–2Mn–Nb and from ~ 15 μm to about 30 μm for Ti–48Al–2Mn–Nb + 15 wt % HfC. Constant velocity, 1100 K, compression tests were then conducted on annealed specimens to gauge the effect of grain size on the elevated temperature strength, and the true compressive stress–strain diagrams from these experiments are presented in Fig. 7. For both materials, the basic shape of the stress–strain curves is similar to that for the as-HIPed forms (Figs 4b and 5b). While the strength levels at the faster two rates are essentially unaffected by the heat treatment, comparison of the curves indicates that the larger grain-sized aluminides show a definite improvement in properties at $\sim 2 \times 10^{-7}$ s^{-1}.

The effects of heat treatment on the 1100 K flow stress–strain rate characteristics are illustrated in Fig. 8. Contrasting the behaviour of the as-HIPed condition to that after annealing does confirm the interrelationship of grain size, strength and strain rate in both materials, where the larger grain size yields the better strength at lower strain rates. For purposes of documentation, the flow stress–strain rate data were fitted to Equation 1, where appropriate, and the results of this analysis are given in Fig. 8 and Table II.

3.4. Post-test microstructures

Measurement of the 1100 K properties indicated that the heat-treated materials possessed the best potential; hence only the microstructural results for these forms will be presented. Fig. 9a and b illustrate the structures at relatively low magnification levels for both the matrix and composite compressed at a strain rate of $\sim 2 \times 10^{-5}$ s^{-1} to about 8% strain. The grain sizes in

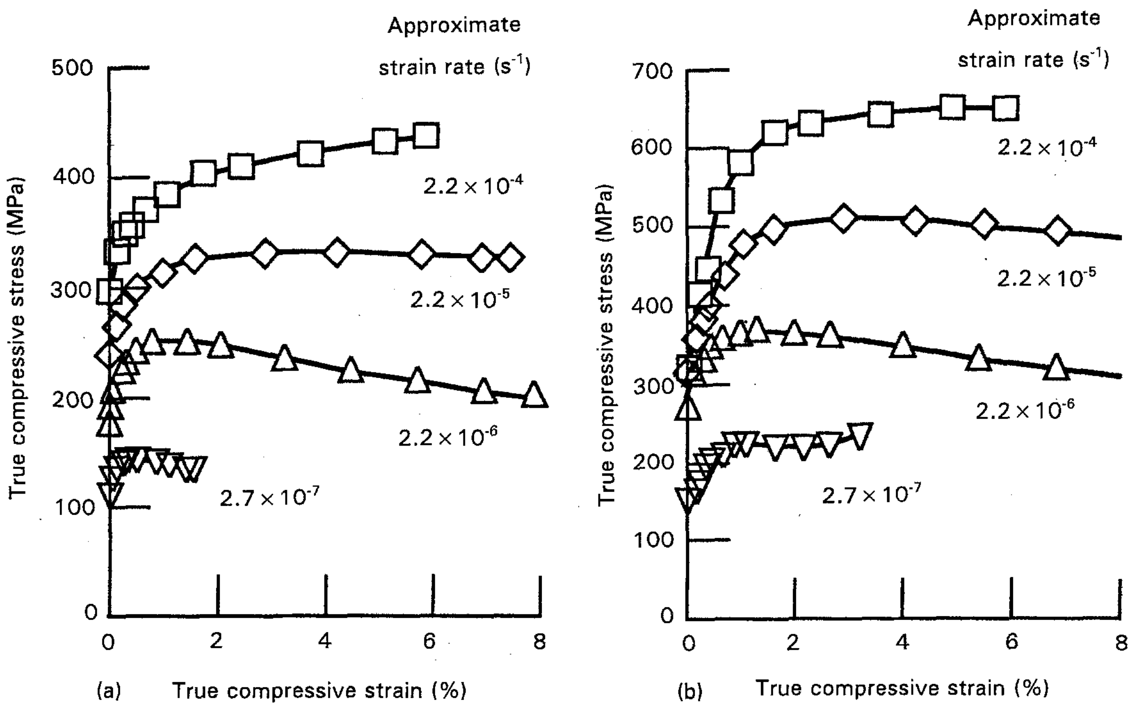

Figure 7 True 1100 K compressive stress–strain diagrams for heat-treated (a) Ti–48Al–2Mn–2Nb and (b) Ti–48Al–2Mn–2Nb + 15 wt % HfC tested under constant velocity conditions.

TABLE II (a) Power law and (b) temperature-compensated power-law fits of the flow stress–strain rate data for Ti–48Al–2Mn–2Nb and Ti–48Al–2Mn–2Nb + 15 wt % HfC

(a)

Material	Condition	Temperature (K)	A (s^{-1})	n	R_d^2	δ_n
Ti–48Al–2Mn–2Nb	As-HIPed	1000	3.45×10^{-37}	11.9	0.999	0.35
		1100	4.14×10^{-25}	7.92	0.998	0.33
Ti–48Al–2Mn–2Nb	Annealed 48 h, 1573 K	1100	7.82×10^{-33}	11.0	0.994	0.87
Ti–48Al–2Mn–2Nb + 15 wt % HfC	Annealed 48 h, 1573 K	1100	2.07×10^{-31}	9.73	0.994	0.73

(b)

Material	B (s^{-1})	n	Q ($kJ\,mol^{-1}$)	R_d^2	δ_n	δ_Q ($kJ\,mol^{-1}$)
Ti–48Al–2Mn–2Nb	5.22×10^3	3.13	352	0.991	0.41	39.7
Ti–48Al–2Mn–2Nb + 15 wt % HfC	6.08×10^2	2.93	332.2	0.952	0.46	37.4
Ti–50.3Al [9][a]	2.15×10^{-3}	3.99	273.5	0.992	0.18	10.7
Ti–48.7Al–2.2W [9][a]	6.59×10^{-4}	4.82	318.8	0.979	0.58	83.8

[a] Reported parameters were determined by simultaneous regression fits over temperature and stress of the steady-state creep data given in [9] and slightly differ from the authors' values.

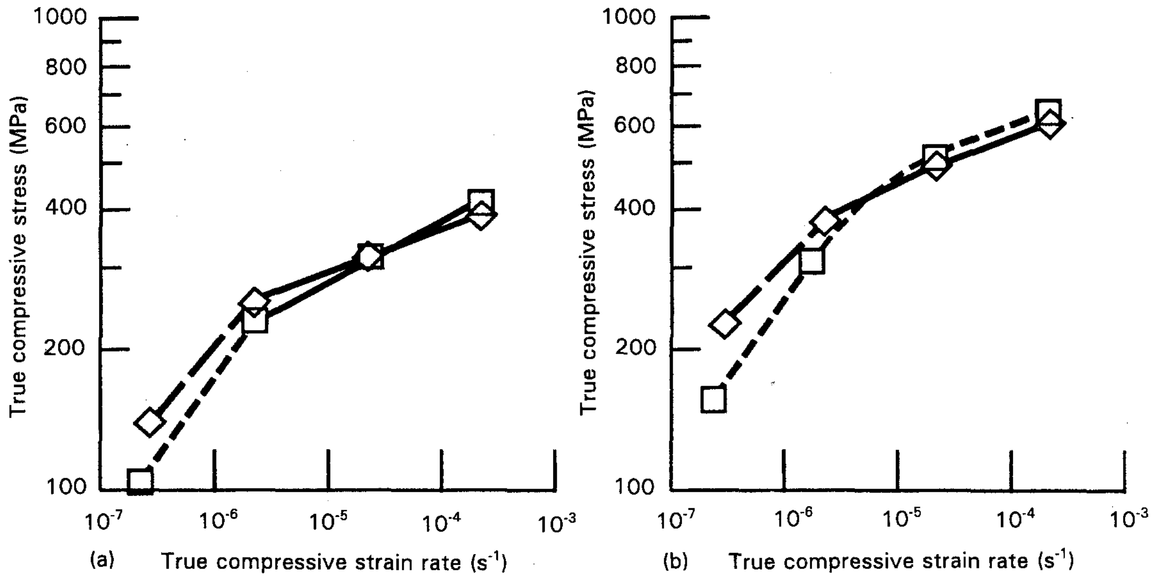

Figure 8 True 1100 K flow stress–strain-rate behaviour for (□) as-HIPed and (◇) heat-treated (a) Ti–48Al–2Mn–2Nb and (b) Ti–48Al–2Mn–2Nb + 15 wt % HfC.

these micrographs are similar to those found in the as-heat-treated-materials, and through comparison with the Fig. 1a and c these figures show the nominal doubling of grain size that was promoted by the 1573 K annealing. Except for the change in grain dimensions, neither heat treatment nor relatively fast 1100 K testing appeared to affect the observed phases or their morphology in either material.

To attempt to understand the cause for the enhanced strength of Ti–48Al–2Mn–Nb + 15 wt % HfC over that of Ti–48Al–2Mn–Nb, samples of both materials which were compressed at $\sim 3 \times 10^{-7}\ s^{-1}$ were examined in the TEM, and typical micrographs are presented in Fig. 9c and d. The most dramatic difference in the heat-treated and tested structures is the high density of small Ti_3Al precipitates within gamma grains in the composite (Fig. 9d) as opposed to virtually precipitate-free grains in the unreinforced matrix (Fig. 9c). Surprisingly, examination of as-HIPed materials after slow strain rate 1100 K testing did not reveal a significant difference in morphology between the matrix and composite, with both compressed materials containing distributions of a small number of fine Ti_3Al particles within gamma grains. In terms of dislocation structure, monolithic Ti–48Al–2Mn–Nb, which had been deformed $\sim$ 1.5% (Fig. 9c) demonstrated significant dislocation activity; while individual dislocations could be seen in

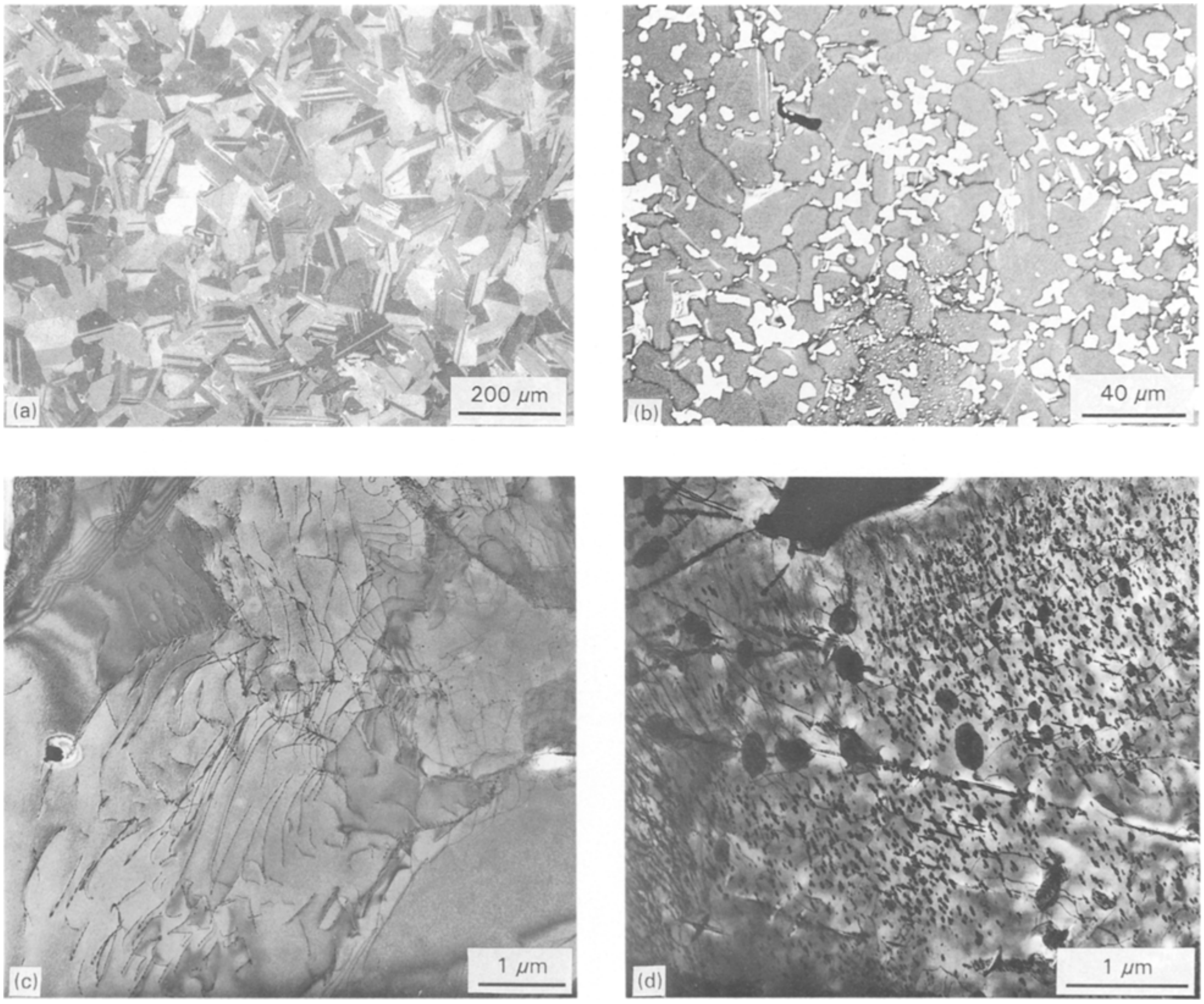

Figure 9 Microstructure of heat-treated and 1100 K compression-tested (a,c) Ti–48Al–2Mn–2Nb and (b, d) Ti–48Al–2Mn–2Nb + 15 wt % HfC. (a) Polarized light optical photomicrograph, (b) scanning electronmicrograph, (c,d) transmission electronmicrographs.

the composite (Fig. 9d) which was compressed to 3%, little evidence of networks was visible.

4. Discussion

The elevated temperature mechanical property data for as-HIPed Ti–48Al–2Mn–Nb and Ti–48Al–2Mn–Nb + 15 wt % HfC clearly indicate that the composite (Fig. 6b) has superior strength in comparison to the matrix (Fig. 6a). Detailed study of the as-HIPed materials revealed that the composite was composed of several second phases (a Hf, Mn-rich compound and a Ti, Al, Hf, Mn carbide) within γ and α_2, where both matrix phases also contained hafnium and probably carbon. The microstructure of Ti–48Al–2Mn–Nb, on the other hand, simply consisted of a mixture of $\gamma + \alpha_2$. Because (1) TEM examination of both as-HIPed materials after slow-rate 1100 K compression testing revealed similar structures (small Ti_3Al particles in gamma grains as illustrated in Fig. 9d), and (2) the stress exponent and activation energy in Table II are practically identical for the two forms, it would appear that the slow plastic flow deformation mechanism is the same in both as-HIPed materials. Hence the primary factor inducing creep resistance in the composite is probably solid-solution strengthening due to carbon [1] and hafnium, rather than the presence of the second-phase particles.

The elevated-temperature strength of either Ti–48Al–2Mn–Nb or Ti–48Al–2Mn–Nb + 15 wt % HfC can be improved via heat treatments which promote grain growth (Fig. 8). In this case, TEM study of both aluminides after slow-rate 1100 K compression testing (Fig. 9c and d) revealed different structures; specifically the composite contained a distribution of small Ti_3Al particles in γ grains, while the γ grains of the unreinforced matrix were free of precipitates. These results indicate that an increase in grain size will enhance creep properties; furthermore, a comparison of the TEM findings for the unreinforced matrix in the as-HIPed and annealed conditions seems to signify that Ti_3Al particles within gamma are not very effective creep-strengthening agents. Extension of this latter contention to the composite augments the hypothesis that the HfC-modified material derives its strength from solid-solution effects instead of second-phase particles.

With the assumption that the flow stress data for the highest temperature/slowest strain-rate regimes (defined by dashed lines in Fig. 6) accurately reflect

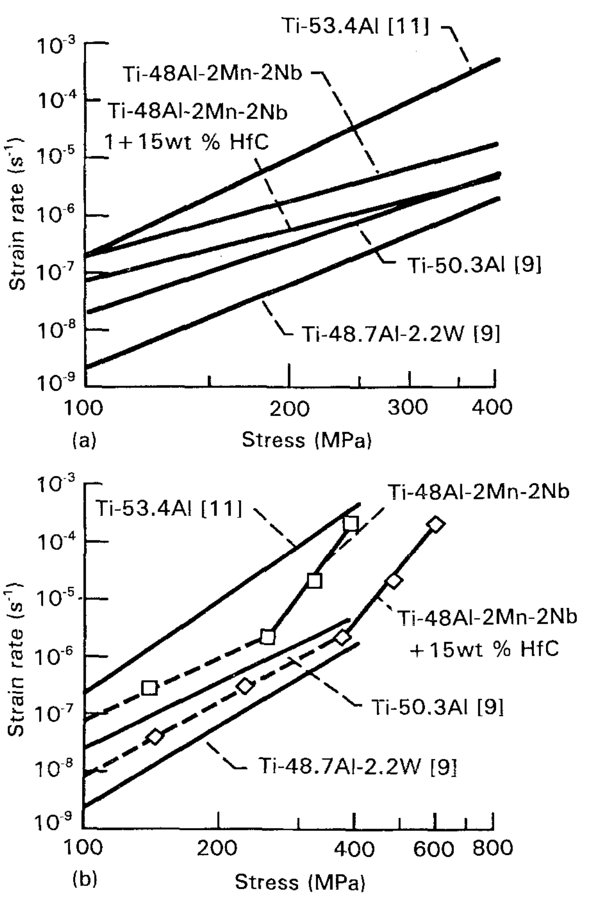

Figure 10 Comparison of the flow strength–strain-rate behaviour of several TiAl-based materials at 1100 K. (a) As-HIPed and (b) after being annealed for 48 h at 1573 K.

creep-type deformation processes for each as-HIPed material, the stress exponents and activation energies (Table II) can be compared to those determined for other TiAl-based materials. For example, values of n of about 3 for the Ti–48Al–2Mn–Nb matrix materials are intermediate to stress exponents reported by Martin *et al.* [9] and Kampe *et al.* [10]. The former group found stress exponents of 4 and 4.8 for creep in the partially lamellar Ti–50.3Al intermetallic and tungsten-particle strengthened Ti–48.7Al–2.2W composite (Table II), while Kampe *et al.* [10] have recently reported stress exponents ranging from ~ 2–3.5 for duplex (lamellar + equiaxed) and equiaxed Ti–48Al and XD^{tm} Ti–48Al + 6 vol % TiB_2 composites. Compared to discrepancies in the measured stress exponents, general agreement exits on the activation energy for creep. Q for the both Ti–48Al–2Mn–Nb materials (Table II) is about 340 kJ mol^{-1} which is in good agreement with measurements from other investigations, such as 318 kJ mol^{-1} for Ti–48.7Al–2.2W (Table II), 340 kJ mol^{-1} for Ti–48Al and XD^{tm} Ti–48Al + 6 vol % TiB_2 composites [10], 330 kJ mol^{-1} for Ti–53.4Al [11], and 355 kJ mol^{-1} for Ti–48Al–2Cr–2Nb [12]. Thus it appears that deformation in TiAl-based materials is a lattice diffusion-controlled process; however, the present stress-exponent data are insufficient to determine the rate-limiting step for dislocation motion.

Although the deformation parameters for the as-HIPed Ti–48Al–2Mn–Nb and Ti–48Al–2Mn–Nb + 15 wt % HfC are generally similar to other TiAls, these materials at present have little to offer in terms of useful elevated-temperature strength. This can be seen in Fig. 10a which compares the 1100 K flow stress–strain rate characteristics for several titanium aluminides. Clearly the deformation resistance of the composite is inferior to both Martin *et al.*'s [9] binary and tungsten particle-strengthened aluminides and is only moderately better than single-phase Ti–53.4Al of Takahashi *et al.* [11]. As demonstrated in Fig. 10b, a grain-growth heat treatment can improve the situation. After 48 h at 1573 K the strength of Ti–48Al–2Mn–Nb + 15 wt % HfC exceeds those of both single-phase alloys, but Martin *et al.*'s particle-strengthened Ti–48.7Al–2.2W still possess the best behaviour. In view of the effect of heat treatment on strength at low strain rates, it is possible that an annealing schedule could be developed which would substantially increase the creep resistance of the HfC-modified material, and render it a worthwhile structural alloy.

5. Conclusion

The intention of this work was to produce materials with an $\alpha_2 + \gamma$ matrix by RST methods, and both the unreinforced Ti–48Al–2Mn–Nb and Ti–48Al–2Mn–Nb + 15 wt % HfC composite have such matrices. While the composite does contain several second phases within the matrix, none was identified to be HfC. The elevated-temperature strengths of the HfC-modified aluminide are superior to those of the matrix, and the best 1100 K temperature slow strain-rate properties in both materials were achieved after high-temperature annealing which yielded larger gamma grain diameters. Examination of the microstructures after deformation in combination with the measured stress exponents and activation energies suggests that creep resistance is due to solid-solution strengthening rather than the presence of second phases.

Acknowledgement

J.D.W. and S.C.F. thank W. McCort for the light optical metallographay and R. Ortiz and P. Book for the additional SEM investigation.

References

1. YOUNG-WON KIM: in "High Temperature Ordered Intermetallic Alloys IV", edited by L. A. Johnson, D. P. Pope and J. O. Steigler, Material Research Society Proceedings 213 (MRS, Pittsburgh, PA, 1991) pp. 777–94.
2. G. E. ALLEN, G. A. CHAMPAGNE, H. L. KLEIN and L. F. SCHULMEISTER, "Benefit of Advanced Materials in Future High Speed Civil Transport Propulsion Systems", NASA CR 185246, July 1990.
3. J. B. ANDREWS and H. D. KESSLER, *J. Metals* **8** (1956) 1348.
4. T. TSUJIMOTO and K. HASHIMOTO, in "High Temperature Ordered Intermetallic Alloys III", edited by C. T. Lui, A. I. Taub, N. S. Stoloff and C. C. Koch, Material Research Society Proceedings 133 (MRS, Pittsburgh, PA, 1989) pp 391–96.
5. S. C. JHA and R. RAY, *J. Mater. Sci. Lett.* **7** (1988) 285.

6. S. C. JHA, R. RAY and J. D. WHITTENBERGER, *Mater. Sci. Eng.* **A119** (1989) 103.
7. J. DANIEL WHITTENBERGER, *ibid.* **57** (1983) 77.
8. *Idem, ibid.* **73** (1985) 87.
9. P. L. MARTIN, M. G. MENDIRATTA and H. A. LIPSITT, *Met. Trans.* **14A** (1983) 2170.
10. S. L. KAMPE, J. D. BRYANT and L. CHRISTODOULOU, *ibid.* **22A** (1991) 447.
11. T. TAKAHASHI, H. NAGAI and H. OIKAWA, *Mater. Sci. Eng.* **A114** (1989) 13.
12. D. S. SHIH and G. K. SCARR, in "High Temperature Ordered Intermetallic Alloys IV", edited by L. A. Johnson, D. P. Pope and J. O. Steigler, Material Research Society Proceedings 213 (MRS, Pittsburgh, PA, 1991) pp. 727–32.

Received 8 April 1992
and accepted 6 September 1993